Water-Soluble Fe(II)−H₂O Complex with a Weak O−H Bond Transfers a Hydrogen Atom via an Observable Monomeric Fe(III)−OH

Lisa M. Brines,[†] Michael K. Coggins,[†] Penny Chaau Yan Poon,[†] Santiago Toledo,[†] Werner Kaminsky,[†] Martin L. Kirk,[‡] and Julie A. Kovacs*,[†]

[†]Department of Chemistry, University of Washington, Campus Box 351700, Seattle, Washington 98195-1700, United States
[‡]Department of Chemistry and Chemical Biology, University of New Mexico, Albuquerque, New Mexico 87131, United States

S *Supporting Information*

ABSTRACT: Understanding the metal ion properties that favor O−H bond formation versus cleavage should facilitate the development of catalysts tailored to promote a specific reaction, e.g., C−H activation or H₂O oxidation. The first step in H₂O oxidation involves the endothermic cleavage of a strong O−H bond (BDFE = 122.7 kcal/mol), promoted by binding the H₂O to a metal ion, and by coupling electron transfer to proton transfer (PCET). This study focuses on details regarding how a metal ion's electronic structure and ligand environment can tune the energetics of M(HO−H) bond cleavage. The synthesis and characterization of an Fe(II)−H₂O complex, **1**, that undergoes PCET in H₂O to afford a rare example of a monomeric Fe(III)−OH, **7**, is described. High-spin **7** is also reproducibly generated via the addition of H₂O to
$\{[Fe^{III}(O^{Me2}N_4(tren))]_2\text{-}(\mu\text{-}O)\}^{2+}$ (**8**). The O−H bond BDFE of Fe(II)−H₂O (**1**) (68.6 kcal/mol) is calculated using linear fits to its Pourbaix diagram and shown to be 54.1 kcal/mol less than that of H₂O and 10.9 kcal/mol less than that of $[Fe(II)(H_2O)_6]^{2+}$. The O−H bond of **1** is noticeably weaker than the majority of reported $M^{n+}(H_xO−H)$ (M = Mn, Fe; $n+$ = 2+, 3+; x = 0, 1) complexes. Consistent with their relative BDFEs, Fe(II)−H₂O (**1**) is found to donate a H atom to TEMPO•, whereas the majority of previously reported $M^{n+}−O(H)$ complexes, including $[Mn^{III}(S^{Me2}N_4(tren))(OH)]^+$ (**2**), have been shown to abstract H atoms from TEMPOH. Factors responsible for the weaker O−H bond of **1**, such as differences in the electron-donating properties of the ligand, metal ion Lewis acidity, and electronic structure, are discussed.
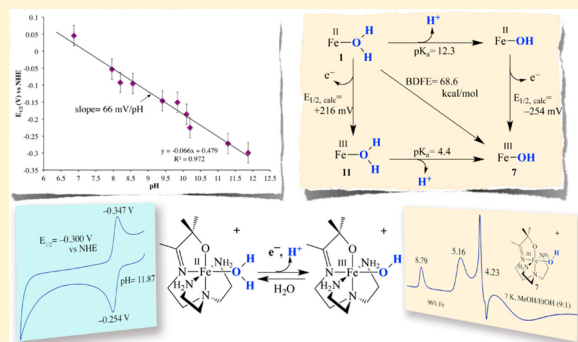
INTRODUCTION

Understanding the mechanism by which Nature drives endothermic H₂O splitting, in order to convert solar energy into storable fuels,[1−3] could provide potential solutions to the global warming/energy crisis.[4−8] The first step in this process involves the endothermic cleavage of an O−H bond of H₂O—a bond which is stronger than the C−H bond of CH₄ (BDFE(HO−H)= 122.7 kcal/mol vs BDFE(H₃C−H) = 96.8 kcal/mol).[9] Although methane is one of the most difficult hydrocarbons to activate, in an appropriate environment, a metal oxo can promote CH₄ C−H bond cleavage via the formation of a strong Fe(O−H) bond.[10] Understanding the metal ion properties that favor O−H bond formation versus O−H bond cleavage is a necessary step toward the development of catalysts tailored to promote a specific reaction, e.g., C−H activation or H₂O splitting. The O−H bonds of water can cleave either heterolytically (H₂O → OH⁻ + H⁺) or homolytically (H₂O → OH• + H•) to afford protons or hydrogen atoms, respectively. Charge balance favors the transfer of protons coupled with electrons (PCET) and avoids the necessity for large overpotentials.[11] By coordinating H₂O to a metal ion, the energetics of O−H bond cleavage become more favorable, the reaction is more controlled, and damaging OH• radicals are avoided.[5,6,8,12,13] The photo-

synthetic Mn₄Ca-containing oxygen evolving complex (OEC) takes advantage of this.[1−3] Oxidation of a metal-coordinated water, M−H₂O, involves the removal of an electron from the metal ion and a proton from the coordinated oxygen (M^{n+}−O(H)−H → M^{(n+1)+}−O(H) + H•). Once the metal oxidation state is high enough, the metal-centered orbitals drop below the oxygen orbitals, thereby facilitating the reductive elimination of O₂. Details regarding how the metal ion electronic structure and ligand environment can tune the energetics of homolytic M(O(H)−H) bond cleavage is part of the focus of the study herein. Examples of M^{n+}−O(H)−H → M^{(n+1)+}−O(H) + H• transformations in well-characterized small molecules are rare.[14−17] The reverse reaction involving metal−oxoo- or metal−hydroxo-promoted H-atom abstraction and concomitant O−H bond formation is more commonly observed[14,18−21] and typically more difficult to promote.

Metal−oxo- or metal−hydroxo-promoted C−H bond cleavage represents a key step in the transformation of hydrocarbons to more useful chemical feedstocks, both in Nature and in the laboratory, and is driven via the formation of strong O−H bonds.

For example, cytochrome P450[22−25] and methane monooxygenases (MMO)[26−28] use either $(L^{\bullet +})Fe(IV)=O$ or $Fe(V)=O$ to abstract H atoms from aliphatic hydrocarbons. Lipoxygenases (LO)[29−31] use M(III)−OH (M = Fe, Mn) to regio- and stereospecifically abstract a H atom from the allylic C−H bond of a fatty acid (BDE ≈ 77 kcal/mol).[32] The LO resting state has been shown to contain a reduced monomeric Fe(II)−H$_2$O in an N$_4$O coordination sphere (Figure 1).[30,33−35] The catalytically
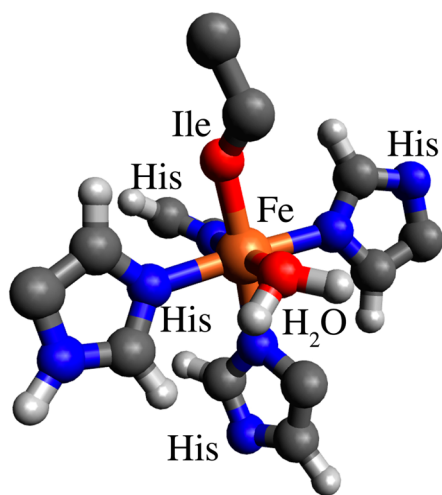

Figure 1. (N$_4$O)Fe(II)−H$_2$O active site of lipoxygenase in its resting state.

active form of LO contains a monomeric Fe(III)−OH (or Mn(III)−OH).[29,36,37] Monomeric Fe(III)−OH species are rare in the absence of H-bond donors and/or a sterically protected cavity.[14,18,38−40] The thermodynamic driving force for M(III)−OH-promoted (M = Fe, Mn) C−H bond oxidation[41−48] depends on the relative strength of substrate X−H (X = C, N, O) versus M(II)(HO−H) (M = Fe, Mn) bonds,[9,49−53] and the latter depends on both the redox potential $(E^0(M^{+3}/M^{+2}))$ and the pK_a of the M(II)(HO−H). As long as the pK_a of M(II)(H$_2$O) is high enough to offset the lower redox potential $E^0(M^{+3}/M^{+2})$, it is possible for a less oxidizing lower valent metal ion, such as M(III)−OH (M = Fe, Mn), to abstract H atoms.

We recently reported a rare example of a water-soluble monomeric Mn(III)−OH complex, $[Mn^{III}(S^{Me2}N_4(tren))(OH)]^+$ (**2**), which, despite its low redox potential (E^0 = 0.33 V vs NHE at pH= 7), is capable of oxidizing TEMPOH via hydrogen-atom abstraction.[54] Much like the thiolate ligand of P450Fe(IV)=O$^{+\bullet}$, which has been shown to facilitate H-atom abstraction by creating a more basic oxo,[22,23,55−57] the thiolate ligand of **2** is proposed to contribute to its reactivity. Herein we describe the synthesis and properties of a water-soluble, synthetic Fe−LO resting state analogue, Fe(II)−OH$_2$, that displays proton-coupled electron transfer (PCET) and has a stability and reactivity that is the inverse of that of the reduced protonated derivative of **2**, Mn(II)−H$_2$O (**5**).[54]

■ EXPERIMENTAL SECTION

General Methods. All reactions were performed using standard Schlenk techniques under an atmosphere of dinitrogen. Fe(MeCN)$_2$(OTf)$_2$ was prepared according to the literature method.[58] Ferrocenium triflate was prepared from ferrocene and silver triflate. All other reagents were obtained from Aldrich Chemical Co. and used without further purification. Solvents were purified through standard procedures. IR spectra were obtained as KBr pellets and recorded on a

PerkinElmer 1700 FTIR. EPR spectra were obtained using either a Varian CW-EPR spectrometer or a Bruker EleXsys EPR spectrometer (purchased with NIH grant #S10-RR023065) at 7 K equipped with an Oxford helium cryostat. Cyclic voltammograms were recorded in MeCN with Bu$_4$N(PF$_6$) (0.100 M) or in 0.01 M aqueous phosphate buffer with 0.100 M KClO$_4$ supporting electrolyte using either a 263A EG&G Princeton Applied Research potentiostat with a glassy carbon working electrode, an SCE reference electrode, and a platinum auxiliary electrode, or a CH Instruments (CHI600E) potentiostat with a glassy carbon working electrode, an Ag/AgCl reference electrode, and a platinum auxiliary electrode. Electronic absorption spectra were recorded using a Hewlett-Packard 8453 diode array spectrometer. Magnetic susceptibility data were acquired using a Quantum Design SQUID Magnetometer and by Evans' Method as modified for a superconducting solenoid.[59,60] Temperatures were obtained using Van Geet's method.[61] Elemental analyses were performed by Galbraith Laboratories (Knoxville, TN) or Atlantic Microlab, Inc. (Norcross, GA).

Preparation of [Fe^{II}(O^{Me2}N$_4$(tren))(H$_2$O)](OTf) (1). Sodium methoxide (216 mg, 4.00 mmol), 3-hydroxy-3-methyl-2-butanone (408 mg, 4.00 mmol), tris(2-aminoethyl)amine (tren) (585 mg, 4.00 mmol), and Fe(MeCN)$_2$(OTf)$_2$ (1.74 g, 4.00 mmol) were dissolved in 15 mL of methanol, and the solution was allowed to stir overnight. All volatiles were then removed in vacuo to afford a canary yellow solid. The crude yellow solid was recrystallized from MeCN/Et$_2$O (1:3), and the obtained solid was then washed with Et$_2$O (3 × 15 mL) and THF (3 × 5 mL) to afford analytically pure **1**. Yield: 907 mg (50.1% yield). Single crystals suitable for X-ray diffraction were grown by vapor diffusion of ether into a saturated methanolic solution of the complex at room temperature. Electronic absorption spectrum (MeCN), λ_{max} (nm) (ε (M^{-1} cm^{-1})): 368 (683). Magnetic moment (solid state): 4.99 μ_B. Magnetic moment (CD$_3$OD, 300.2 K): 5.00 μ_B. IR: ν(OH/OD) = 3488/2508 cm^{-1}, ν(C=N) = 1671 cm^{-1}. Anal. Calcd for **1** (FeC$_{12}$H$_{27}$N$_4$O$_5$SF$_3$): C, 31.87; H, 6.02; N, 12.39. Found: C, 31.48; H, 5.86; N, 12.20.

Preparation of [μ-OH-(Fe^{III}(O^{Me2}N$_4$(tren))$_2$](OTf)$_3$ (9). Ferrocenium triflate (167 mg, 0.5 mmol) was added to an acetonitrile (15 mL) solution of **1** (217 mg, 0.5 mmol). The solution was stirred overnight at room temperature and evaporated to dryness, and the residue was washed with ether (3 × 10 mL). The remaining solid was redissolved in MeOH (5 mL), layered with ether (15 mL), and cooled overnight to yield golden yellow needles of **9** (180 mg, 69.6% yield). Single crystals of **9**·MeOH·Et$_2$O suitable for X-ray analysis were grown by vapor diffusion of ether into a methanolic solution of the complex. Electronic absorption spectrum (MeCN), λ_{max} (nm) (ε (M^{-1} cm^{-1})): 238 (10 200), 313 (5540). IR ν(OH/OD) = 3462/2526 cm^{-1}, ν(C=N) = 1670 cm^{-1}. Magnetic moment (CD$_3$OD, 298.0 K): 3.78 μ_B/Fe. Anal. Calcd for **9**·MeOH (Fe$_2$C$_{26}$H$_{55}$N$_8$O$_{12}$S$_3$F$_9$·CH$_3$OH): C, 29.28; H, 5.20; N, 10.51. Found: C, 29.88; H, 5.24; N, 10.36.

Preparation of [μ-O-(Fe^{III}(O^{Me2}N$_4$(tren)))$_2$](OTf)$_2$ (8). A methanolic (15 mL) solution of **1** (296 mg, 0.65 mmol) was stirred in air at room temperature overnight. The solution was reduced in volume (5 mL), layered with ether (10 mL), and allowed to stand overnight at −40 °C to yield brown solid **8** (180 mg, 31.1% yield). Single crystals suitable for X-ray analysis were grown by vapor diffusion of ether into a methanolic solution of the complex. Electron absorption spectrum (MeCN), λ_{max} (nm) (ε (M^{-1} cm^{-1})): 231 (13 200), 332 (10 100), 464 (sh, 910), 494 (825). IR ν(C=N) = 1680 cm^{-1}. Magnetic moment (CD$_3$CN, 297.8 K): 1.72 μ_B/Fe. Anal. Calcd for **8** (Fe$_2$C$_{24}$H$_{50}$N$_8$O$_9$S$_2$F$_6$): C, 32.59; H, 5.70; N, 12.67. Found: C, 32.50; H, 5.74; N, 12.57.

Determination of the pK_a of [Fe^{III}(O^{Me2}N$_4$(tren))(H$_2$O)]$^{2+}$. Hydroxide-bound $[Fe^{III}(O^{Me2}N_4(tren))(OH)]^+$ (**7**) was generated in situ via the addition of 1 equiv (5 mg, 0.03 mmol) of TEMPO$^\bullet$ to a 3.0 mM solution of $[Fe^{II}(O^{Me2}N_4(tren))(H_2O)](OTf)$ (**1**) (14 mg, 0.03 mmol) in 10 mL of H$_2$O. This aqueous solution of **7** was then titrated with 10 μL (0.1 equiv) aliquots of a 300 mM HOTf solution (3 mmol in 10 mL of H$_2$O) until subsequent additions of acid no longer resulted in a noticeable change (at 1.3 equiv; Table S-1, Supporting Information) to the measured solution pH. pH measurements were made using a Beckman Coulter 400 series hand-held meter. Full reversibility was

Table 1. Crystal Data, Intensity Collections, and Structure Refinement Parameters for [Fe^{II}(O$^{Me}_2$N$_4$(tren))(H$_2$O)](OTf) (1), [μ-OH-(Fe^{III}(O^{Me2}N$_4$(tren)))$_2$](OTf)$_3$·MeOH·Et$_2$O (9), and [μ-O-(Fe^{III}(O^{Me2}N$_4$(tren)))$_2$](OTf)$_2$ (8)

	1	9	8
formula	FeN$_4$O$_5$C$_{12}$H$_{27}$F$_3$S	Fe$_4$N$_{16}$O$_{25.66}$C$_{54.66}$H$_{114.64}$F$_{18}$S$_6$	Fe$_2$N$_8$O$_9$C$_{24}$H$_{50}$F$_6$S$_2$
MW	452.29	2164.45	884.54
T, K	130(2)	130(2)	130(2)
unit cell	triclinic	monoclinic	Cubic
a, Å	9.4900(2)	20.5150(3)	22.6100(5)
b, Å	9.9290(3)	13.0900(2)	22.6100(5)
c, Å	10.8760(3)	18.6110(3)	22.6100(5)
α, deg	100.5110(11)	90	90
β, deg	98.0540(11)	111.6420(7)	90
γ, deg	99.3920(15)	90	90
V, Å^3	978.74(5)	4645.51(12)	11558.5(4)
Z	2	2	12
d(calcd), g/cm^3	1.535	1.548	1.511
space group	P1	P2$_1$/c	I2$_1$3
R	0.0457	0.0541	0.0521
R$_w$	0.125	0.1714	0.1192
GOF	1.137	1.032	1.016

checked by back-titration of the resulting solutions using a 0.1 M aqueous KOH solution. pK_a values were determined from the average inflection point of the titration curves obtained from three independent experiments.

Determination of the pK_a of [Fe^{II}(O^{Me2}N$_4$(tren))(H$_2$O)](OTf) (1). An aqueous 3.0 mM solution of **1** (14 mg, 0.03 mmol) was titrated with 10 μL (0.04 equiv) aliquots of a 120 mM solution of KOH (1.2 mmol in 10 mL H$_2$O) until subsequent additions of base no longer resulted in a noticeable change (at 1.28 equiv; Table S-2, Supporting Information) to the measured solution pH. pH measurements were made using a Beckman Coulter 400 series hand-held meter. Full reversibility was checked by back-titration of the resulting solution using a 0.1 M aqueous HOTf solution. The pK_a value determined was the average inflection point of the titration curves obtained from three independent experiments.

Reduction of TEMPO• by 1. This reaction was most readily examined using EPR spectroscopy. In a typical experiment, 350 μL of a 0.1 M solution of TEMPO was prepared in MeCN/tol (9:1) and placed within an EPR tube in a drybox. One equivalent of **1** (from a 0.1 M (44 mg in 1 mL MeCN) stock solution) was then added in 0.25 equiv aliquots (88 μL) to the TEMPO solution. The resulting mixture was frozen in liquid nitrogen, and an EPR spectrum was recorded.

X-ray Crystallography. A clear crystal plate of **1** was cut down to 0.36 × 0.34 × 0.31 mm and mounted on a glass capillary with oil. Data was collected at −143 °C with four sets of exposures. Crystal-to-detector distance was 30 mm, and exposure time was 10 s per degree for all sets. The scan width was 2°. Data collection was 94.5% complete to 28.28° and 98.7% complete to 25° in ϑ. A total of 37 364 partial and complete reflections was collected covering the indices $h = -10$ to 12, $k = -13$ to 11, $l = -13$ to 14. There were 4603 reflections that were symmetry independent, and $R_{int} = 0.0819$ indicated that the data was of slightly less than average quality (0.07). Indexing and unit cell refinement indicated a monoclinic P lattice. The space group was found to be P$\bar{1}$ (No. 2).

An orange prism of [μ-O-(Fe^{III}(O^{Me2}N$_4$(tren)))$_2$](OTf)$_2$·MeOH·Et$_2$O (**8**), size 0.52 × 0.31 × 0.14 mm, was mounted on a glass capillary with oil. Data was collected at −143 °C with four sets of exposures. Crystal-to-detector distance was 30 mm, and exposure time was 20 s per degree for all sets. The scan width was 1.6°. Data collection was 95.7% complete to 28.33° and 98.7% complete to 25° in ϑ. A total of 96 888 partial and complete reflections were collected covering the indices $h = -27$ to 27, $k = -16$ to 17, $l = -24$ to 24. There were 11 099 reflections that were symmetry independent, and $R_{int} = 0.0377$ indicated that the data was excellent (average quality 0.07). Indexing and unit cell refinement indicated a monoclinic P lattice. The space group was found to be P2$_1$/c (No. 14).

A brownish black crystal plate of μ-OH-[Fe^{III}(O^{Me2}N$_4$(tren))]$_2$-(OTf)$_3$ (**9**) was cut down to 0.41 × 0.30 × 0.26 mm and mounted on a glass capillary with oil. Data was collected at −143 °C with two sets of exposures. Crystal-to-detector distance was 30 mm, and exposure time was 30 s per degree for all sets. The scan width was 2°. Data collection was 88.8% complete to 29.87° and 99.0% complete to 25° in ϑ. A total of 36 608 partial and complete reflections were collected covering the indices $h = -31$ to 31, $k = -31$ to 31, $l = -31$ to 31. There were 4752 reflections that were symmetry independent, and $R_{int} = 0.069$ indicated that the data was of average quality (0.07). Indexing and unit cell refinement indicated a cubic I lattice. The space group was found to be I2$_1$3 (No. 199).

For **1**, **8**, and **9**, the data was integrated and scaled using hkl-SCALEPACK. Solution by direct methods (SIR97) produced a complete heavy atom phasing model. All non-hydrogen atoms were refined anisotropically by full-matrix least-squares. All hydrogen atoms were located using a riding model. Crystallographic data is contained in Table 1, and selected bond distances and angles are contained in Table 2.

RESULTS AND DISCUSSION

Synthesis and Properties of [Fe^{II}(O^{Me2}N$_4$(tren))(H$_2$O)]-(OTf) (1). The six-coordinate monomeric complex [Fe^{II}(O^{Me2}N$_4$(tren))(H$_2$O)](OTf) (**1**) was prepared via a Schiff-base condensation between 3-hydroxy-3-methyl-2-butanone and tris(2-aminoethyl)amine (tren) in the presence of Fe(MeCN)$_2$(OTf)$_2$ in MeOH. The use of an iron source without coordinating anions (i.e., iron triflate)[58] was essential in order to avoid the formation of anion-bridged (e.g., Cl$^-$) ferrous species. Like the resting state of the lipoxygenase enzyme (Figure 1),[62] complex **1** is high spin (S= 2), both in the solid state (μ_{eff} = 4.99 μ_B) and in solution (μ_{eff}(300.2 K) = 5.00 μ_B in CD$_3$OD). The incorporation of a water molecule into the sixth coordination site of [Fe^{II}(O^{Me2}N$_4$(tren))(H$_2$O)]$^+$ (**1**) was shown by X-ray crystallography (Figure 2). Although the origin of the water molecule is not known, **1** reproducibly forms (based on ESI/MS (Figure S-1, Supporting Information), quantitative UV/vis (Figure S-2, Supporting Information), IR, and crystallographic unit cell parameters). Potential sources of H$_2$O include either the water released in the metal-templated Schiff-base condensation reaction or incomplete drying of the solvent. A water molecule is presumed to be coordinated to the lipoxygenase iron site, based on its geometry, although it was not directly observed in the

Table 2. Selected Bond Distances (Angstroms) and Bond Angles (degrees) for [Fe^{II}(O^{Me2}N$_4$(tren))(H$_2$O)](OTf) (1), [Fe^{III}(O^{Me2}N$_4$(tren))]$_2$-(μ-O)(OTf)$_2$ (8), and [Fe^{III}(O^{Me2}N$_4$(tren))]$_2$-(μ-OH)(OTf)$_3$ (9)

	1	8	9
Fe–O(1)	2.001(2)	1.915(3)	1.869(3)
Fe–N(1)	2.129(2)	2.162(3)	2.114(5)
Fe–N(2)	2.257(2)	2.305(3)	2.244(4)
Fe–N(3)	2.249(2)	2.187(3)	2.125(5)
Fe–N(4)	2.222(2)	2.168(4)	2.124(5)
Fe(1)–O(2)^a	2.149(2)	1.8115(18)	2.023(3)^c
Fe(2)–O(2)^a	N/A	1.8115(18)	2.019(3)^c
Fe(1)···Fe(2)	N/A	3.314^b	3.695
O(1)–Fe–N(1)	76.49(6)	76.70(12)	77.62(17)
O(1)–Fe–N(2)	153.14(6)	151.24(12)	152.77(16)
O(1)–Fe–N(3)	105.45(6)	103.47(13)	104.56(17)
O(1)–Fe–N(4)	108.00(6)	104.90(13)	106.00(17)
N(1)–Fe–N(3)	94.77(6)	87.92(13)	92.73(18)
N(1)–Fe–N(4)	103.51(7)	92.15(14)	96.92(18)
N(3)–Fe–N(4)	144.73(7)	150.85(14)	149.26(16)
O(1)–Fe–O(2)^a	103.44(6)	100.63(12)	93.56(14)^c
N(1)–Fe–O(2)^a	175.84(6)	176.87(15)	170.90(16)^c
Fe(1)–O(2)–Fe(2)	N/A	132.4(2)^b	132.11(16)^c

^{a}O(2) refers to either the bridging oxo (hydroxo) or the coordinated H$_2$O oxygen. ^{b}For this structure the two halves of the "dimer" are related by crystallographic symmetry so that Fe(1) = Fe(2). ^{c}For this structure the two halves of the "dimer" are inequivalent; therefore, the irons (Fe(1) and Fe(2)) are inequivalent. For comparative purposes, the bridging hydroxo oxygen (O(14)) for this structure is labeled O(2) in the table.
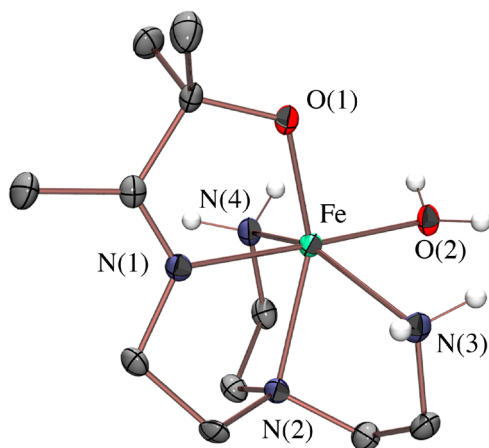
Figure 2. ORTEP of [Fe^{II}(O^{Me2}N$_4$(tren))(H$_2$O)]$^+$ (1) with most of the hydrogen atoms omitted for clarity.

crystal structure.[30,33,34,63] Complex **1** therefore supports the viability of this assumption. The infrared spectrum of **1** (Figure S-3, Supporting Information), crystallized from MeCN or MeOH, reproducibly shows an ν_{O-H} stretch at 3488 cm^{-1}, which shifts to 2508 cm^{-1} upon the addition of D$_2$O (Figure S-4, Supporting Information). This shift (980 cm^{-1}) is close to that predicted (950 cm^{-1}) for an ν_{O-H} based on Hooke's law for a simple harmonic oscillator. Although water is usually assumed to be a fairly labile ligand, the coordinated water of soybean 1-LO is not displaced by either ethanol or HCN analogous to the behavior of our model **1**.[35]

The average Fe–N bond length in **1** (2.21 Å; Table 2) is analogous to that of the LO resting state (Fe–N$_{His}$(avg) = 2.2

Å).[33,34] The iron–alkoxide bond (2.001 (2) Å) is slightly shorter than the enzyme Fe–O$_{Ile}$ bond (2.1 Å), and the Fe–OH$_2$ bond length (2.149 (2) Å) falls in the expected range (2.103(3)–2.159(9) Å).[58,64–67] Examples of crystallographically characterized Fe(II)–H$_2$O complexes include [Fe(H$_2$O)$_6$](OTf)$_2$,[58] Fe$_3$(4-isopropyl-1,2,4-triazole)$_6$(H$_2$O)$_6$)(tosylate)$_6$,[66] and Fe-(II)(TPP)(CCl$_2$)(H$_2$O).[67] In contrast to **1** (Figure 2), our previously reported Mn analogue [Mn^{II}(S^{Me2}N$_4$(tren))(H$_2$O)]$^+$ (**5**) was found to be unstable with respect to spontaneous H$_2$O loss and formation of five-coordinate [Mn^{II}(S^{Me2}N$_4$(tren))]$^+$ (**4**).[54] Similarly, the thiolate-ligated derivative of **1**, [Fe^{II}(S^{Me2}N$_4$(tren))]$^+$ (**6**),[68–71] was shown to remain five coordinate, with no evidence for the binding of a sixth ligand, even in coordinating solvents. The increased affinity for a sixth ligand, seen upon replacement of the thiolate of **6** with the alkoxide of **1**, indicates that the Fe^{2+} ion of **1** is more Lewis acidic than either the Fe^{2+} or the Mn^{2+} ion of thiolate-ligated **6** and **4**,[72] respectively. The more electron-withdrawing character of the alkoxide vs thiolate ligand, as well as periodic trends in metal ion radii, would predict this. A more Lewis acidic metal ion should decrease the pK_a of the coordinated H$_2$O (vide infra). The additional electron of d^6 Fe^{2+} introduces e$^-$/e$^-$ repulsion, not present in d^5 Mn^{2+}, making it easier to oxidize (vide infra) and thus serve as a H-atom donor.

Oxidation of 1 in Water via PCET. Water-bound [Fe^{II}(O^{Me2}N$_4$(tren))(H$_2$O)](OTf) (**1**) displays a pH-dependent Fe$^{II/III}$ oxidation potential in H$_2$O with a slope in the Pourbaix diagram (66 mV/pH; Figure 3) close to that expected (59 mV/
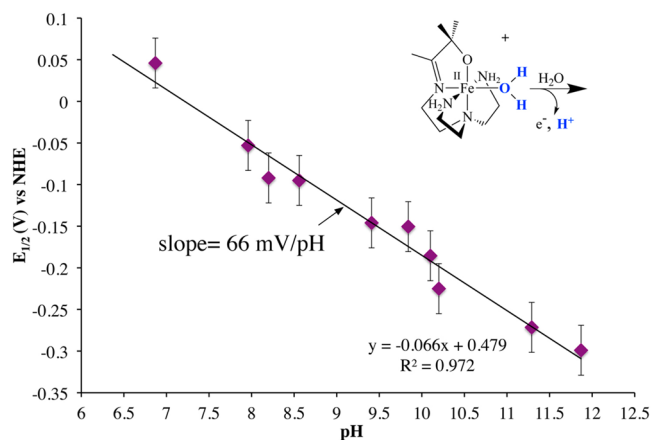

Figure 3. Pourbaix diagram for [Fe^{II}(O^{Me2}N$_4$(tren))(OH$_2$)]$^+$ (**1**) in buffered H$_2$O at 298 K. pH was tuned by adding a few drops of dilute aqueous H$_2$SO$_4$ or NH$_4$OH to a buffered aqueous solution of **1**. Potentials shown are relative to NHE (0.1 M KClO$_4$ supporting electrolyte, 100 mV s^{-1} scan rate).

pH) for ideal Nernstian behavior. This redox behavior is indicative of the transfer of a single proton per electron (i.e., a proton-coupled redox process, PCET). Structurally analogous [Mn^{III}(S^{Me2}N$_4$(tren))(OH)]$^+$ (**2**) also displays PCET in aqueous solution.[54] The product of proton-coupled oxidation of **1** in H$_2$O would be hydroxo-ligated [Fe^{III}(O^{Me2}N$_4$(tren))-(OH)]$^+$ (**7**, Scheme 1). Although we could not isolate **7**, it is reproducibly generated in situ in protic solvents (wet MeOH and H$_2$O), as demonstrated by the presence of a cathodic wave, associated with Fe(III) → Fe(II) conversion, in the cyclic voltammogram of **1** (i_a/i_c = 1.0) in H$_2$O (Figure 4) as well as the reproducible observation of an intense EPR signal (g = 8.79, 5.16, 4.23; wet MeOH/EtOH glass; Figure 5) that accounts for 96% of
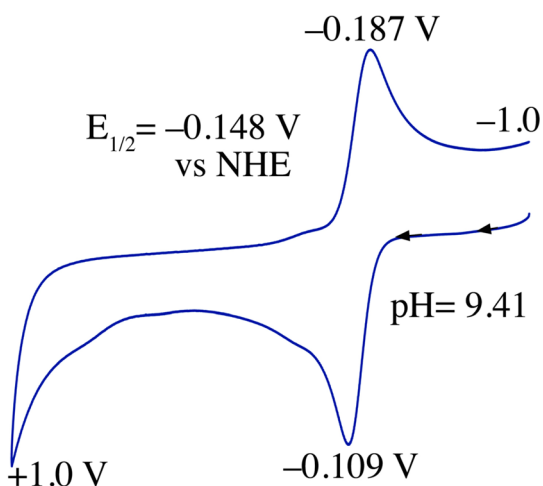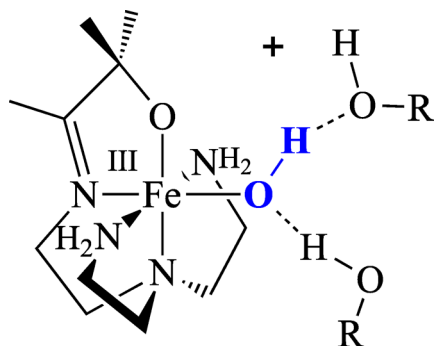
Scheme 1

$E_{1/2} = -0.148$ V
vs NHE

–0.187 V

–1.0

+1.0 V   –0.109 V

pH= 9.41

Figure 4. Cyclic voltammogram of $[Fe^{II}(O^{Me2}N_4(tren))(H_2O)]^+$ (**1**) in H_2O at pH = 9.41 and 298 K vs NHE (0.1 M KClO$_4$ supporting electrolyte, 50 mV s^{-1} scan rate).
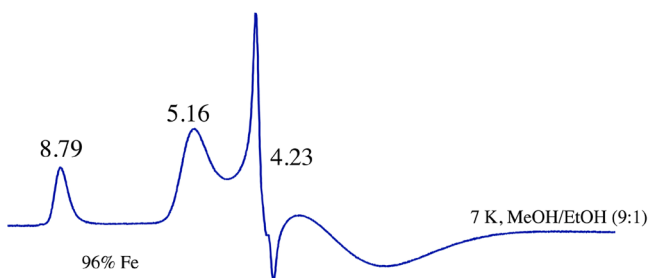

8.79   5.16   4.23

96% Fe

7 K, MeOH/EtOH (9:1)

Figure 5. X-band EPR spectrum of $[Fe^{III}(O^{Me2}N_4(tren))(OH)]^+$ (**7**), generated via the addition of TEMPO to **1** (5 mM), at 7 K in wet MeOH/EtOH (9:1) glass. Frequency =9.424 GHz, power =2.00 mW, modulation frequency =10, time constant =81.92 ms. The signal was quantified using a 5 mM FeCl$_3$ standard, and was integrated using Simfonia.

the iron. On the basis of the scan rate (50 mV/s) and sweep width of the cyclic voltammogram (Figure 4), the oxidized Fe(III) hydroxo compound, $[Fe^{III}(O^{Me2}N_4(tren))(OH)]^+$ (**7**), has a lifetime of at least 46 s in aqueous solution at ambient temperatures. Monomeric Fe(III)−OH complexes are extremely rare[39,73,74] but can be stabilized by H bonds (and steric bulk), consistent with the fact that **7** can only be generated in wet protic solvents. In the few reported Fe(III)−OH examples,[39,73,74] H-bonding donors are built into the ligand system. In H_2O or MeOH, the hydroxo of **7** would be surrounded by a sphere of H-bond donors (Scheme 1) that should also be capable of

stabilizing a monomeric Fe(III)−OH. In aprotic MeCN, on the other hand, chemical oxidation of **1** by Cp_2Fe^+ affords an EPR silent species, containing an even number of antiferromagnetically coupled Fe(III) ions (vide infra), indicating that a monomeric structure is not favored in the absence of a H-bonding solvent.

The potential at which Fe(II)−OH$_2$ (**1**) and Fe(III)−OH (**7**) interconvert in H_2O at pH = 7 (E^0 = 17 mV vs NHE; Figure 3) is 327 mV lower than that at which Mn(II)−OH$_2$ (**5**) and Mn(III)−OH (**2**) interconvert (E^0 = +344 mV vs NHE at pH = 7). This is not surprising given that Mn(II) complexes typically have higher redox potentials (by as much as 1 V) than their structurally analogous Fe(II) derivatives.[14,68,75−77] Destabilizing e^-/e^- repulsion forces present in the doubly occupied t$_{2g}$ orbital of a d^6, but not in a d^5, ion make it easier to remove an electron from Fe(II) vs Mn(II) as is reflected in their lower redox potentials. The thiolate ligand of **2** provides some stability to Mn(III), thus explaining the relatively small (<1 V) potential difference $E(Mn^{3+/2+})−E(Fe^{3+/2+})$ for **1** vs **2**. The lower redox potential of **1** relative to **2** indicates that Fe(III)−OH (**7**) should be less oxidizing and therefore less capable of abstracting H atoms from substrates than Mn(III)−OH (**2**).[54] Conversely, this indicates that Fe(II)−H$_2$O (**1**) contains weaker O−H bonds relative to Mn(II)−H$_2$O (**5**) (vide infra) and should thus be capable of acting as a H-atom donor.

Formation of Oxo-Bridged Fe(III)−O−Fe(III) and Its Protonated Fe(III)−O(H)−Fe(III) Derivative. The manganese analogue of Fe(III)−OH (**7**), Mn(III)−OH (**2**),[54] was obtained previously via the proton-induced cleavage of bimetallic oxo-bridged $\{[Mn^{III}(S^{Me2}N_4(tren))]_2$-$(\mu$-O)$\}^{2+}$ (**3**) in H_2O.[78] Oxo-bridged **3** was obtained via O_2 addition to the corresponding Mn(II) precursor $[Mn^{II}(S^{Me2}N_4(tren))]^+$ (**4**). Exploring this as an alternative route to **7** would support the assumption that the aqueous PCET reaction of Figure 3 generates an Fe(III)−OH species analogous to Mn(III)−OH (**2**).[54] Dioxygen addition to Fe(II)−H$_2$O (**1**) in MeCN was, in fact, found to afford a binuclear oxo-bridged species, $\{[Fe^{III}(O^{Me2}N_4(tren))]_2$-$(\mu$-O)$\}^{2+}$ (**8**), the structure of which was verified by X-ray crystallography (Figure 6). Monooxo-bridged **8** can also be synthesized via the addition of PhIO to **1** in MeCN at −40 °C. Intermediates are not observed in either of these reactions, even when they are carried out at low-temperatures. Like its manganese analogue, Mn(III)−μ-O−Mn(III) (**3**), the oxo bridge of $\{[Fe^{III}(O^{Me2}N_4(tren))]_2$-$(\mu$-O)$\}^{2+}$ (**8**) can be proto-

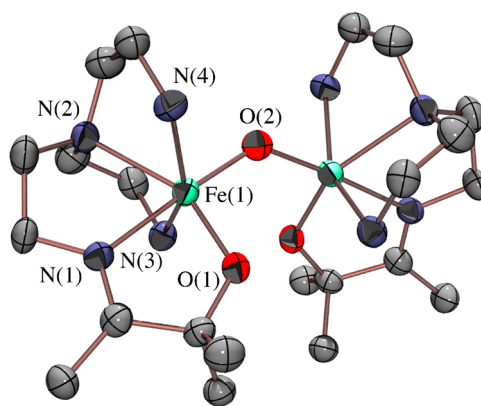
N(4)   O(2)

N(2)

Fe(1)

N(1)   N(3)   O(1)

Figure 6. ORTEP drawing of the cation of **8** showing 50% probability ellipsoids and atom-labeling scheme. Hydrogen atoms on all carbons have been omitted for clarity.

nated with noncoordinating acids, e.g., HBF_4 (Figures S5–S8, Supporting Information). However, in sharp contrast to **3**,[78] protonation of **8** does not result in bridge cleavage, is fully reversible in MeCN (Scheme 2), and affords a binuclear

Scheme 2
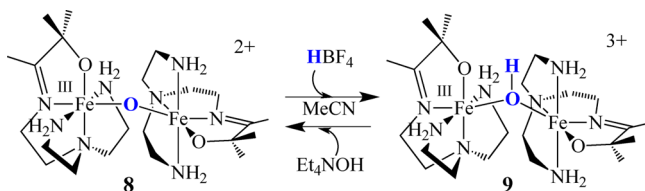
hydroxo-bridged species $[\mu$-OH-$(Fe^{III}(O^{Me2}N_4(tren)))_2]$-$(OTf)_3$ (**9**) containing a stable unsupported Fe(III)−O(H)−Fe(III) core as determined by X-ray crystallography (Figure S-9, Supporting Information). Metrical parameters for **8** and **9** are compared in Table 2. To date, **8** and **9** represent the only reported set of crystallographically characterized protonated and deprotonated nonheme, μ-O(H)-bridged ferric dimers lacking additional bridging ligands. In MeCN, oxo-bridged **8** can be regenerated via the addition of base (NH_4OH) to hydroxo-bridged **9** (Scheme 2, Figure S-6, Supporting Information). Weaker acids (e.g., H_2O and MeOH) do not protonate **8**, at least in MeCN. This contrasts with the acid/base chemistry of dimanganese **3**, where the oxo was shown to be readily protonated by MeOH (to afford $[Mn^{III}(S^{Me2}N_4(tren))$-$(OMe)]^+$),[54] implying that the oxo of **8** is less basic than that of **3**. The thiolate ligand of $\{[Mn^{III}(S^{Me2}N_4(tren))]_2$-$(\mu$-O)$\}^{2+}$ (**3**) likely contributes to a more basic oxo. This role for a thiolate ligand is proposed to be responsible for the P450 Fe(IV) oxo intermediate's ability to abstract H atoms from strong C−H bonds.[22,23,55−57]

In MeCN solution, the ambient-temperature magnetic moment of oxo-bridged $\{[Fe^{III}(O^{Me2}N_4(tren))]_2$-$(\mu$-O)$\}^{2+}$ (**8**; μ_{eff} = 1.72/Fe) is significantly less than that of hydroxo-bridged $[\mu$-OH-$(Fe^{III}(O^{Me2}N_4(tren)))_2]^{3+}$ (**9**; μ_{eff} = 3.78/Fe), indicating that antiferromagnetic coupling present in **8** decreases upon protonation. This is supported by variable-temperature magnetic susceptibility data (2−300 K; 1 T) in the solid state. In H_2O, on the other hand, the magnetic moment (μ_{eff} = 5.85 μ_B) is consistent with an isolated S = 5/2 spin system, indicating that cleavage of the oxo bridge occurs (vide infra). The best fits to the data for **8** (Figure S-10, Supporting Information) and **9** (Figure 7; solid red line) using the van Vleck expression and the exchange Hamiltonian $H = -2J(S_1 \cdot S_2)$ show that the coupling constant decreases substantially (J = −174 cm^{-1} (g = 1.98) for **8** to J = −9.7 cm^{-1} (g = 1.99) for **9**) upon protonation as one would expect.[80−83]

Hydroxo-bridged $[\mu$-OH−$(FeIII(O^{Me2}N_4(tren)))_2]^{3+}$ (**9**) is also obtained upon Cp_2Fe^+ oxidation of $[Fe^{II}(O^{Me2}N_4(tren))$-$(H_2O)]^+$ (**1**) in MeCN, a reaction which is in contrast to both the Cp_2Fe^+-induced oxidation of thiolate-ligated $[Fe^{II}(S^{Me2}N_4$-$(tren))]^+$ (**6**) in MeCN, which affords solvent-bound $[Fe^{III}(S^{Me2}N_4(tren)(MeCN))]^{+2}$,[84] and the oxidation chemistry of **1** in H_2O, which affords Fe(III)−OH (**7**). A plausible mechanism for the Cp_2Fe^+-induced conversion of **1** to **9** in aprotic MeCN is as follows. One would expect oxidation of Fe(II)−H_2O^+ (**1**) to a more Lewis acidic Fe(III)−H_2O^{2+} to cause the pK_a of the coordinated H_2O to decrease dramatically, thus favoring its deprotonation, as supported by the PCET behavior shown in the aqueous Pourbaix diagram of Figure 3.
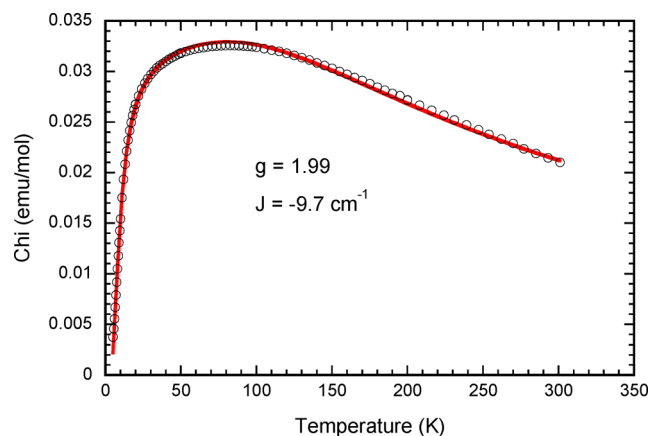

Figure 7. Variable-temperature (2−300 K) magnetic susceptibility data for hydroxo-bridged **9** in an applied magnetic field of 1 T.

This would afford $[Fe^{III}(O^{Me2}N_4(tren))(OH)]^+$ (**7**), which in aprotic solvents is transient and undergoes a condensation reaction to afford **8** (and an equivalent of H_2O) as demonstrated by EPR, vide supra. In the presence of acidic Fe(III)−H_2O^{2+} or H_3O^+, protonation of the oxo bridge of **8** would be favored, resulting in the formation of **9**.

Electrochemical and Spectroscopic Evidence for the Conversion of Fe(III)(μ-O)Fe(III) (8) to Fe(III)−OH (7) in H_2O. In protic solvents such as H_2O and wet MeOH monomeric Fe(III)−OH (**7**) is less transient than in MeCN, as demonstrated by the electrochemical and EPR experiments of Figures 4 and 5. In H_2O, the equilibrium **7** ⇆ **8** + H_2O lies far to the left, in part because the excess H_2O (55.5 M) increases the rate of the back-reaction relative to the forward reaction but also because **7** is stabilized via H bonds to solvent (Scheme 1), which creates a larger activation barrier to the condensation reaction **7** → **8** + H_2O. That the reverse reaction **8** + H_2O → **7** is favored in H_2O is demonstrated by the fact that (a) an identical reversible cyclic voltammogram is obtained for both Fe(III)−O−Fe(III) (**8**) in H_2O ($E_{1/2}$ = 10 mV vs NHE; pH = 7) and Fe(II)−H_2O (**1**) ($E_{1/2}$ = 17 mV vs NHE; pH = 7) in H_2O, (b) an identical UV−vis spectrum is obtained upon dissolution of Fe(III)−O−Fe(III) (**8**) in H_2O (λ_{max} = 274 nm; Figure S-11, Supporting Information) and upon the addition of TEMPO$^\bullet$ (vide infra) to Fe(II)−H_2O (**1**) in H_2O (λ_{max} = 274 nm; Figure S-12, Supporting Information), (c) the addition of H_2O (240 equiv) to Fe(III)−O−Fe(III) (**8**) in MeCN causes the electronic absorption band at λ_{max}= 332 nm characteristic of **8** to be replaced by a new intense band at λ_{max} = 282 nm (Figure S-13, Supporting Information), and (d) an intense EPR signal identical to that of $[Fe^{III}(O^{Me2}N_4(tren))(OH)]^+$ (**7**) (Figure 5) is observed when **8** is dissolved in wet MeOH/EtOH (9:1) (Figure S-14, Supporting Information). In addition, reduction of Fe(III)−O−Fe(III) (**8**) in H_2O is proton coupled, as shown by the Pourbaix diagram of Figure 8, and the equation governing this fully reversible PCET process, $E_{pH} = E^0(pH = 0) − (49\ mV/pH) \cdot pH = +355\ mV − (49\ mV/pH) \cdot pH$, is the same, within error, as that of the Pourbaix diagram of Fe(II)−H_2O (**1**; Figure 3). The electrochemical and chemical reversibility of this process on the CV time scale (∼25 s) rules out the possibility that monomeric $[Fe^{II}(O^{Me2}N_4(tren))(H_2O)]^+$ (**1**) and binuclear $\{[Fe^{III}(O^{Me2}N_4(tren))]_2$-$(\mu$-O)$\}^{2+}$ (**8**) are interconverting during the electrochemical experiment. One would expect dimerization to be particularly slow compared to proton-coupled electron transfer, especially in the presence of 55.5 M H_2O (vide
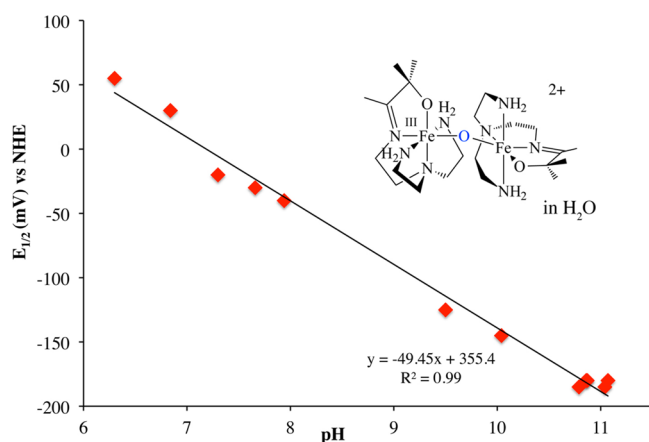
Figure 8. Pourbaix diagram for Fe(III)(μ-O)Fe(III) (**8**) in H_2O at 298 K. pH was tuned using dilute aqueous solutions of either HBF$_4$ or NH$_4$OH (0.1 M KClO$_4$ supporting electrolyte, 100 mV s^{-1} scan rate). Potentials shown are relative to NHE.

supra) and at the 1 mM Fe concentration used for the CV experiment. In summary, the data described above indicates that binuclear **8** converts to monomeric **7** in the presence of excess H_2O (Scheme 3). Analogous behavior is seen with binuclear oxo-bridged Mn(III)(μ-O)Mn(III) (**3**), which converts to monomeric Mn(III)−OH (**2**) upon dissolution in H_2O.[54]

Scheme 3
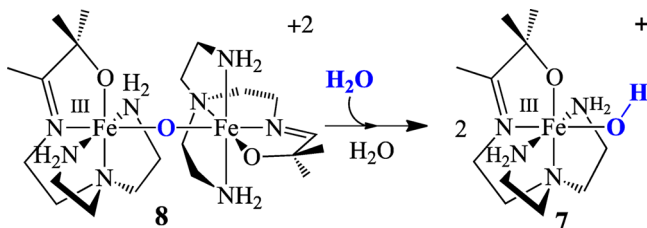
Bond Dissociation Free Energy, pK_a, and Reactivity of Fe(II)−H_2O (1) with TEMPO.

The bond strength of a metal-coordinated water M(II)(HO−H) can be related to both the redox potential (E^0(M$^{3+/2+}$) and the M(II)(HO−H) pK_a according to the Bordwell eq 2[49,50] below

$$\mathrm{BDFE}(M(II)(HO - H))$$
$$= 23.06E^0(M^{3+/2+}) + 1.37(pK_a) + C_{G,sol} \quad (2)$$

where $C_{G,sol}$ is the solvent-dependent energy of formation and solvation of H$^\bullet$ in a given solvent ($C_{G,H2O}$ = 57.6 kcal/mol; $C_{G,MeCN}$ = 54.9 kcal/mol). The metal ion properties that influence O−H bond strengths affect the two key parameters, E^0(M$^{3+/2+}$) and pK_a, in opposite ways. An increase in metal ion Lewis acidity, for example, tends to decrease the pK_a of a coordinated H_2O but increases the redox potential E^0(M$^{3+/2+}$). The former would weaken the O−H bond, whereas the later would strengthen the O−H bond, relative to a less Lewis acidic metal ion. Details regarding how the metal ion's electronic structure and ligand environment can tune the energetics of M(HO−H) bond cleavage are part of the focus of the study herein. In H_2O, the energy cost of both the proton-transfer and the electron-transfer steps of O−H bond cleavage are included in the electrochemical data. This is because the two events cannot be separated in this solvent, as shown by the pH-dependent

redox potential of [Fe^{II}(O^{Me2}N$_4$(tren))(H_2O)]$^+$ (**1**) (Figure 3). Using the information provided in the Pourbaix diagram of Figure 3, one can directly calculate the O−H bond dissociation free energy (BDFE) for **1** using the modified form[9] of the Bordwell equation[49,50] (eq 3 below)

$$\mathrm{BDFE}(M^{II}(HO - H))$$
$$= 23.06[E_{pH}] + 1.37(pH) + 57.6 \, \mathrm{kcal/mol} \quad (3)$$

where E_{pH} is the redox potential of **1** at a given pH and the constant 57.6 kcal/mol is the solvent-dependent energy of formation and solvation ($C_{G,H2O}$) of H$^\bullet$ in H_2O. Redox potentials (E_{pH}) for this calculation are referenced to NHE according to convention[9] and obtained using a least-squares fit to the data of Figure 3. On the basis of this calculation, the O−H BDFE for **1** in H_2O was determined to be 68.6 kcal mol^{-1} (Figure 9; Table 3).
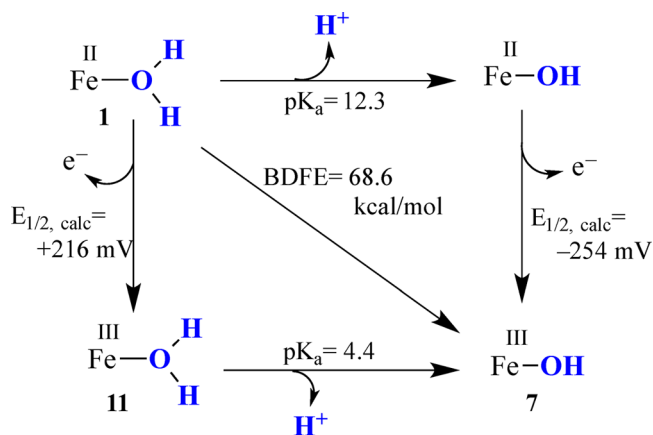

Figure 9. Thermochemical cycle for [Fe^{II}(O^{Me2}N$_4$(tren))(H_2O)]$^+$ (**1**)-promoted PCET reactions in aqueous solution, where $E_{pH} = E^0$(pH= 0) − 66 mV/pH*pH = +479 mV − 66 mV/pH*pH (vs NHE) is obtained from fits to the data for the Pourbaix diagram of Figure 3.

This O−H bond is 54.1 kcal/mol weaker than that of free H_2O (122.7 kcal/mol),[9] demonstrating that binding to an Fe^{2+} ion significantly activates the O−H bond toward homolytic cleavage. In part, this reflects the fact that the Fe−OH product is significantly more stable than a hydroxyl radical HO$^\bullet$.

One can separate the proton-transfer energy cost involved in cleaving the O−H bond from the electron-transfer energy cost by determining the pK_a of either Fe(II)−H_2O (**1**) or Fe(III)−H_2O (**11**), as illustrated by the thermodynamic cycle of Figure 9. Titration of **1** (0.030 mmol) with 0.04 equiv aliquots of KOH (10 μL of a 120 mM aqueous solution) in H_2O (Figure 10, Table S-1, Supporting Information) and Fe(III)−OH (**7**), generated in situ via the addition of TEMPO$^\bullet$ to **1**, with HOTf (Figure 11, Table S-2, Supporting Information) afforded a pK_a = 12.3 for Fe(II)−H_2O (**1**) and a pK_a = 4.4 for Fe(III)−H_2O (**11**) in H_2O. This experimental pK_a data indicates that the acidity of H_2O (pK_a= 15.7) increases by 3 orders of magnitude upon coordination to Fe(II), making heterolytic (as well as homolytic) O−H bond cleavage favorable. Oxidation of Fe(II) to Fe(III) increases the acidity of the coordinated water by approximately 8 orders of magnitude. Oxidized (tren-N$_4$O^{Me2})Fe(III)−H_2O (**11**; pK_a = 4.4) is an order of magnitude more acidic than oxidized (tren-N$_4$S^{Me2})Mn(III)−H_2O (pK_a = 5.3),[54] consistent with what one would expect based on metal ion Lewis acidity and the electron-withdrawing versus -donating nature of alkoxide and thiolate ligands. The anionic alkoxide and amine ligands of **1** decrease the

Table 3. Thermodynamic Properties of $[Fe^{II}(O^{Me2}N_4(tren))(H_2O)]^+$ (1) and $[Mn^{II}(S^{Me2}N_4(tren))(H_2O)]^+$ (5) versus TEMPOH and the Corresponding Aqueous Complexes in Water

	O−H BDFE (in H₂O, kcal/mol)	pKₐ (in H₂O)	$E_{1/2}$ (in H₂O, pH = 7)[a]	ref
$[Fe^{II}(O^{Me2}N_4(tren))(H_2O)]^+$ (1)	68.6	12.3	+17 mV	this work
TEMPOH	71.0	12.9[b]	−175 mV[c]	9
$[Mn^{II}(S^{Me2}N_4(tren))(H_2O)]^+$ (5)	74.0	d	+344 mV	54
$[Fe(II)(H_2O)_6]^{2+}$	79.5	9.5	+357 mV[e]	9
$[Mn(II)(H_2O)_6]^{2+}$	91.8	11.2	+1.10 V[f]	14

[a]Potentials vs NHE. [b]pKₐ(TEMPOH/TEMPO⁻). [c]E(TEMPO•/TEMPO⁻). [d]Mn(II)−H₂O (5) is too unstable with respect to H₂O loss to measure its pKₐ. [e]Calculated using E^0(pH= 0) − 59 mV/pH*pH = +770 mV − (59 mV/pH)7. [f]Calculated using E^0(pH= 0) − 59 mV/pH*pH = +1510 mV − (59 mV/pH)7.
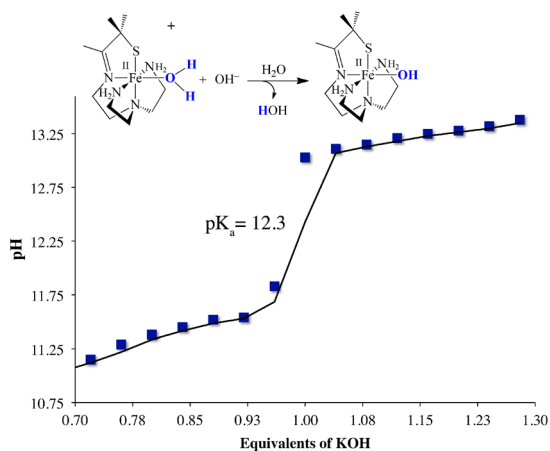
Figure 10. Titration curve for the hydroxide-induced deprotonation of $[Fe^{II}(O^{Me2}N_4(tren))(H_2O)]^+$ (1). pH measurements were made using a Beckman Coulter 400 series hand-held meter.
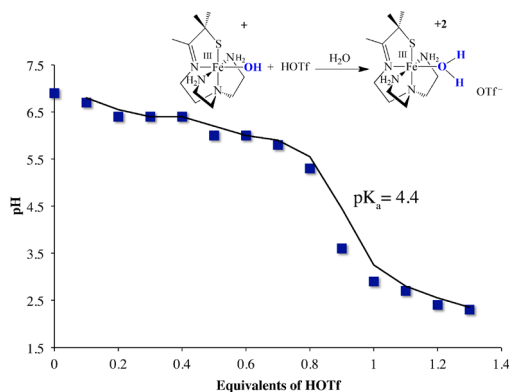
Figure 11. Titration curve for the HOTf-induced protonation of $[Fe^{III}(O^{Me2}N_4(tren))(OH)]^+$ (7) (generated in situ via the addition of TEMPO• to $[Fe^{II}(O^{Me2}N_4(tren))(H_2O)]^+$ (1)) in H₂O). pH measurements were made using a Beckman Coulter 400 series hand-held meter.

acidity of the coordinated H₂O by ∼3 orders of magnitude relative to $[Fe(II)(H_2O)_6]^{2+}$ (pKₐ= 9.5, Table 3).[9] Using the experimentally determined pKₐ values and BDFEs one can calculate estimated redox potentials E^0(Fe(II)H₂O/Fe(III)-H₂O) = +216 mV and E^0(Fe(II)OH/Fe(III)OH) = −254 mV vs NHE using the Bordwell equation (eq 2) and then compare the proton-transfer and electron-transfer energy cost required to cleave the O−H bond. The energy cost of removing an electron from protonated Fe(II)−H₂O (1) is 10.84 kcal/mol (0.470 V· 23.06 kcal mol⁻¹V⁻¹) greater than that required to remove an electron from deprotonated Fe(II)−OH (Figure 9). This makes sense given that the proton would stabilize the additional

electron density on the reduced metal ion of 1. The energy cost of removing a H⁺ from reduced Fe(II)−H₂O (1) (1.37·12.3 = +16.85 kcal/mol) is 10.82 kcal/mol greater than that required to remove a H⁺ from oxidized Fe(III)−H₂O (11) (+6.03 kcal/mol). The larger barrier to removing a H⁺ (16.85 kcal) versus an electron (0.216·23.06 = 4.98 kcal/mol) from 1 indicates that if sequential transfer of e⁻ followed by H⁺ or vice versa were to occur, as opposed to concerted H⁺ + e⁻ = H• (HAT), the latter (i.e, counter clockwise around the thermodynamic cycle of Figure 9) would be more favored.

In order to experimentally verify the calculated O−H bond strength of 1, we examined its reactivity with TEMPO•—an oxidant that favors concerted HAT. This experiment was most successfully carried out in MeCN. As shown by the complete disappearance of the EPR signal associated with TEMPO• (g = 2.01, 1.99, 1.97; Figure 12) upon the addition of 1.0 equiv of 1 (in
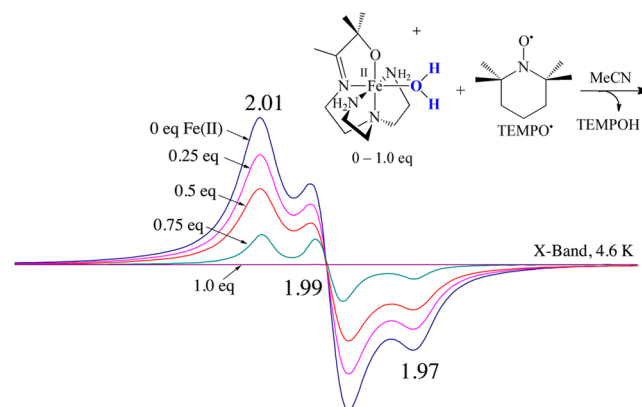
Figure 12. Titration of TEMPO• with 0−1.0 equiv of $[Fe^{II}(O^{Me2}N_4(tren))(H_2O)]^+$ (1) in 0.25 equiv aliquots in MeCN/ toluene as monitored by X-band EPR. This shows that 1.0 equiv of TEMPOH is required.

0.25 equiv aliquots) we can see that TEMPO• does indeed react with Fe(II)−OH₂ (1), consistent with their relative bond dissociation free energies (Table 3). The final Fe³⁺ product is not observed under these conditions since the hydroxo species dimerizes to antiferromagnetically coupled 8 in MeCN (vide supra).

Influence of Metal Ion Coordination Sphere and Electronic Structure on O−H Bond Dissociation Free Energy. By comparing the quantitative BDFE data obtained for $[Fe^{II}(O^{Me2}N_4(tren))(H_2O)]^+$ (1) versus that of other M(O-(H)−H) (M = Fe, Mn) compounds (Table 4), we can examine how the structural and electronic properties of a metal ion tune the energetics of M(HO−H) bond cleavage—the first step in water oxidation. The experiments described above show that

Table 4. O−H Bond Strengths for $[Fe^{II}(O^{Me2}N_4(tren))(H_2O)]^+$ (1) and $[Mn^{II}(S^{Me2}N_4(tren))(H_2O)]^+$ (5) versus TEMPOH, Tyr−OH, H_2O, and Other M(II,III)−(H_2O, OH) (M = Fe, Mn) Complexes

	O−H BDFE kcal/mol	O−H BDE kcal/mol	solvent	ref
$[Fe^{II}(O^{Me2}N_4(tren))(H_2O)]^+$ (1)	68.6	66.8	H_2O	this work
$[Fe^{II}(O^{Me2}N_4(tren))(H_2O)]^+$ (1)	64.7[a]	65.6[a]	MeCN	this work
$[Fe^{II}L(OH)]^{1-}$ (12)[b]	64.1	66	DMSO	14
TEMPOH	71.0	69.2	H_2O	9
TEMPOH	66.5	67.4	MeCN	9
TEMPOH	67.5	72.1	DMSO	9
$[Fe^{II}(H_2O)_6]^{2+}$	79.5	77.7	H_2O	9
$[Fe^{II}PY5(H_2O)]^{2+}$ (19)[c]	75.4	80	DMSO	76
$[Mn^{II}(S^{Me2}N_4(tren))(H_2O)]^+$ (5)	74.0	72.2	H_2O	54
$[Mn^{II}(S^{Me2}N_4(tren))(H_2O)]^+$ (5)	69.6	70.5	MeCN	54
$[Mn^{II}L(OH)]^{1-}$ (13)[c]	72.4	77	DMSO	14
$[Mn^{III}(Me_2EBC)(OH)(H_2O)]^{2+}$ (17)[d]	82.4	83[f]	acetone/H_2O (4:1)	43
$[L'_2Mn^{II}(\mu\text{-}OH)_2Mn^{III}L'_2]^{3+}$ (18)[e]	74.1	75[f]	MeCN	20
$[Mn^{III}Mn^{IV}(\mu\text{-}OH)(\mu\text{-}O)(salpn)_2]$	75.1	76[f]	MeCN	86
$[Mn^{III}Mn^{IV}(\mu\text{-}OH)(\mu\text{-}O)(bpy)_2]$ (16)	85.8	84[f]	H_2O	86
$[Mn^{II}PY5(H_2O)]^{2+}$ (20)[f]	81.1	82	MeCN	77
Tyr-OH	87.8	86.5	H_2O	11, 9
$[Mn^{II}(H_2O)_6]^{2+}$	91.8	90	H_2O	14
P450 cmpd II $Fe^{IV}-OH$	~98	~99	protein cavity	23
$[Fe^{III}L(OH)]^{1-}$ (14)[c]	105.4	110[f]	DMSO	14
$[Mn^{III}L(OH)]^{1-}$ (15)[c]	110.4	115[f]	DMSO	14
H_2O	122.7	120.9	H_2O	9

[a]Itaclicized BDFEs are estimated as described in the text. [b]L= tris[(N′-tert-butylureaylato)-N-ethyl)]aminato. [c]PY5 = 2,6-bis((2-pyridyl)-methoxymethane)pyridine. [d]Me2EBC = 4,11-dimethyl-1,4,8,11-tetraazabicyclo[6.6.2]hexadecane. [e]L′ = 1,10-phenanthroline. [f]Involves a $M^{IV/III}$ as opposed to $M^{III/II}$ couple.

coordination of H_2O to the Fe^{2+} ion of **1** weakens the O−H bond by 54.1 kcal/mol relative to free H_2O. The pentadentate alkoxide/amine ligand weakens the O−H bond by 10.9 kcal/mol relative to an aqueous ligand environment as shown by the relative BDFE of **1** versus $[Fe(II)(H_2O)_6]^{2+}$ (Table 3).[9] Compared to the thiolate-ligated Mn^{2+} derivative $[Mn^{II}(S^{Me2}N_4(tren))(H_2O)]^+$ (**5**),[54] the combination of an alkoxide ligand and Fe^{2+} in $[Fe^{II}(O^{Me2}N_4(tren))(H_2O)]^+$ (**1**) weakens the O−H BDFE by 5.4 kcal/mol (Table 3). In part, this reflects the differences between Mn^{2+} and Fe^{2+}—Mn complexes tend to have stronger O−H bonds than Fe (vide infra, Table 4). The pentadentate thiolate/amine ligand of **5** weakens the O−H bond by 17.8 kcal/mol relative to $[Mn(II)(H_2O)_6]^{2+}$ (Table 3).[14] The bond dissociation free energies for $[Fe^{II}(O^{Me2}N_4(tren))(H_2O)]^+$ (**1**) and $[Mn^{II}(S^{Me2}N_4(tren))(H_2O)]^+$ (**5**) relative to TEMPOH (Table 3) are consistent with the inverse reactions promoted by each (Scheme 4): TEMPO• abstracts a H atom from **1** but not from **5**, and oxidized $[Mn^{III}(S^{Me2}N_4(tren))(OH)]^+$ (**2**) abstracts a H atom from TEMPOH, whereas $[Fe^{III}(O^{Me2}N_4(tren))(OH)]^+$ (**7**) does not. A similar reactivity pattern is seen with previously reported $[M(II)H_3L(OH)]^{1-}$ (M = Fe(**12**), Mn(**13**)) and $[M(III)H_3L(O)]^{1-}$ (M = Fe(**14**), Mn(**15**); L = tris[(N′-tert-butylureaylato)-N-ethyl)]aminato): $[Fe(II)H_3L(OH)]^{1-}$ (**12**) reduces TEMPO• (to afford $[Fe(III)H_3L(O)]^{1-}$), whereas $[Mn(II)H_3L-(OH)]^{1-}$ (**13**) does not.[14] Conversely $[Mn(III)H_3L(O)]^{1-}$ (**15**) oxidizes TEMPOH, whereas $[Fe(III)H_3L(O)]^{1-}$ (**14**) does not.[14] This again is consistent with the relative BDFE of **12**, **13**, and TEMPOH (Table 4). As shown by the representative examples of Table 4, with the exception of anionic $[Fe^{II}L-(OH)]^{1-}$ (**12**), the O−H bond of **1** is noticeably weaker than the majority of reported $M^{n+}(H_xO−H)$ (M = Mn, Fe; n = 2+, 3+; x = 0, 1) complexes.[9,14,20,44,76,85] In contrast to Mn, very few

Scheme 4
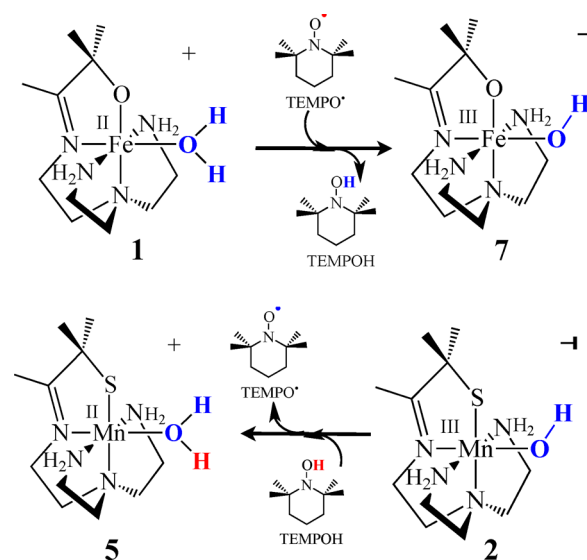
M(HO−H) or M(O−H) BDE have been reported for Fe, however.[21] Inspection of Table 4 shows that for the limited number of available examples, the O−H BDE is greater for $Mn(H_xO−H)$ versus $Fe(H_xO−H)$ (x = 0, 1). With the exception of a few, bond dissociation enthalpies (BDEs), as opposed to bond dissociation free energies (BDFE), were reported, making a direct comparison with our results difficult. As discussed by Mayer[9] and Tilset,[53] it is preferable that entropy effects be included, especially when high-spin metal complexes are involved, making BDFE a more meaningful parameter. We therefore converted the reported bond dissociation enthalpies (BDE) for the complexes included in Table 4 to estimated

BDFEs, for comparative purposes, using the relationship shown in eq 4[9]

$$BDE_{sol} = BDFE_{sol} + (C_{H,sol} - C_{G,sol}) \qquad (4)$$

where $C_{G,sol}$ is the solvent-dependent energy of formation and solvation of H• in a given solvent ($C_{G,H2O}$ = 57.6 kcal/mol; $C_{G,MeCN}$ = 54.9 kcal/mol; $C_{G,DMSO}$ = 71.1 kcal/mol) and $C_{H,sol}$ is the solvent-dependent enthalpy of formation and solvation of H• in a given solvent ($C_{H,H2O}$ = 55.8 kcal/mol; $C_{H,MeCN}$ = 59.4 kcal/mol; $C_{H,DMSO}$ = 75.7 kcal/mol). As shown by eq 4 as well as the extensive tables in Mayer's review,[9] BDFEs tend to vary with solvent, and with the exception of $[Mn^{III}Mn^{IV}(\mu\text{-}OH)(-O)(bpy)_2]^{2+}$ (**16**),[86] $[Fe(II)(H_2O)_6]^{2+}$,[9] **1**, and **5**, most of the BDEs shown in Table 4 were measured in MeCN, DMSO, or acetone/H₂O (4:1) as opposed to H₂O. This also makes a direct comparison with our results difficult. If we assume that the solvation energy of $[Fe^{II}(O^{Me2}N_4(tren))(H_2O)]^+$ (**1**) is identical to that of $[Fe^{III}(O^{Me2}N_4(tren))(OH)]^+$ (**7**) then the difference between the BDFE in H₂O versus MeCN is equal to the difference between the free energy of solvation of H• in water (8.98 kcal/mol) versus in MeCN (5.12 kcal/mol).[9] Using this and eq 2 we estimate that the O−H BDFE for **1** in MeCN is 64.7 kcal/mol. The anionic amide-ligated hydroxo complexes $[Fe(II)L(OH)]^{1-}$ (**12**) and $[Mn(II)H_3L(OH)]^{1-}$ (**13**)[14] have O−H bond dissociation free energies (BDFEs) closest to those of our aquo complexes **1** and **5**, respectively. Both ligands, L = tris[(N′-tert-butylureaylato)-N-ethyl)]aminato) (N_4^{3-}) and $(tren)N_4^{Me2}O^{1-}$, are anionic and therefore electron rich. The other complexes containing neutral ligands are cationic and have stronger O−H bonds by 10.7−14.8 kcal for Fe(II) (relative to **1** in MeCN) and 4.5−22.2 kcal/mol for Mn(II) (relative to **5** in MeCN). As previously noted,[14] an increase in oxidation state (from M^{+2} to M^{+3}) increases O−H BDFEs by 2.7−38 kcal/mol for Mn (Table 4) and 41.3 kcal/mol for Fe. Complexes **12** and **13** are one of a few systems for which BDE data for two different oxidation states M^{+2} and M^{+3} (M = Mn, Fe) in an identical ligand environment are available for comparison (Table 4).[14] A detailed comparison is also available for $[Mn^{III}(Me_2EBC)(OH)(H_2O)]^{2+}$ (**17**) and its reduced protonated derivatives.[43]

For the complexes reported herein as well as others in Table 4, differences in O−H BDFEs can be qualitatively explained as follows. Given that the metal ion Lewis acidity ($\sim Z_{eff}/r$) and electronic structure can tune a metal complex's affinity for H₂O, pK_a(H$_x$OH), and redox potential (E^0), this property is going to be important in determining M(H$_x$O−H) bond strengths (eq 2). Both the smaller ionic radius of Fe(II) versus Mn(II) as well as the electron-withdrawing versus electron-donating properties of the alkoxide versus thiolate ligand contribute to an increased Lewis acidity of **1** relative to **5** as shown by its greater affinity for H₂O.[54] The influence of the alkoxide ligand alone is demonstrated by the more direct comparison between $[Fe^{II}(O^{Me2}N_4(tren))(H_2O)]^+$ (**1**) which binds H₂O and $[Fe^{II}(S^{Me2}N_4(tren))]^+$ (**6**) which does not. The stronger metal ion Lewis acidity of **1** versus **5** also decreases the pK_a of the M(O(H)−H) in **1**, which weakens the O−H bond toward both heterolytic as well as homolytic cleavage. The pairing of d electrons in **1** (d⁶) but not **5** (d⁵) lowers the redox potential (E^0) of **1** relative to **5**, and this also weakens the O−H bond in Fe(II)−H₂O (**1**) relative to Mn(II)−H₂O (**5**). Molecular charge influences the two parameters that are key to determining O−H BDFE, pK_a, and $E_{1/2}$, in opposite ways. The cationic molecular charge of $[Fe^{II}(PY5)(OH_2)]^{2+}$ (**19**)[76] (Table 4), for example, decreases the pK_a of the coordinated H₂O, relative to anionic

$[Fe(II)L(OH)]^{1-}$ (**12**),[14] but raises the redox potential relative to anionic **12** (E^0(**12**) = −1.79 V, E^0(**19**) = −85 mV vs Fc$^{+/0}$ in MeCN).[14,76] The former would weaken the O−H bond, whereas the latter would strengthen it. Although the pK_a of **12** was not reported, that (pK_a = 25)[14] of oxidized $[Fe(III)L(OH)]^{1-}$ (**14**) (which should be lower than that of **12**) is significantly greater than that of **19** (pK_a = 8.1).[76] One can conclude therefore that differences in ligand architecture and donor properties, metal ion Lewis acidity and electronic structure, and molecular charge and symmetry can be responsible for weakening the O−H bond of H₂O by as much as 54 kcal/mol (with **1**) or as little as ∼13 kcal/mol (with **15**).

■ SUMMARY AND CONCLUSIONS

Herein we report the synthesis and structure of an Fe(II)−H₂O complex, $[Fe^{II}(O^{Me2}N_4(tren))(H_2O)]^+$ (**1**), with weak O−H bonds (BDFE = 68.6 kcal/mol) that undergoes PCET (66 mV/pH) in H₂O and transfers H atoms to TEMPO• to afford a rare example of a monomeric ferric hydroxide (g = 8.79, 5.16, 4.23), $[Fe^{III}(O^{Me2}N_4(tren))(OH)]^+$ (**7**). Comparison of the quantitative BDFE data obtained for Fe(II)−H₂O (**1**) versus that of other M(O(H)−H) (M = Fe, Mn) compounds allowed us to qualitatively determine how the coordination environment and electronic structure of a metal ion can tune the energetics of M(HO−H) bond cleavage—the initial step of water oxidation. Coordination to the Fe²⁺ ion of **1** was shown to weaken the O−H bond of H₂O by 54.1 kcal/mol, and the pentadentate alkoxide ligand was shown to weaken the O−H bond by 10.9 kcal/mol relative to the aqueous ligand environment of $[Fe(II)(H_2O)_6]^{2+}$. A tabulation of reported O−H bond strengths in $M^{n+}(H_xO−H)$ (M = Mn, Fe; n+ = 2+, 3+; x = 0, 1) complexes showed that Mn complexes appear to have a higher energy cost in the first step of H₂O splitting than Fe (Table 4). The higher Lewis acidity of Fe²⁺ relative to Mn²⁺ and relief of e⁻/e⁻ repulsion upon oxidation of Fe²⁺ contributes to a weaker Fe(II)(O(H)−H) bond relative to Mn(II)(O(H)−H) by decreasing the redox potential (E^0) and pK_a for Fe and increasing its affinity for H₂O. Despite the more favorable energetics with Fe, it is likely that the photosynthetic oxygen-evolving complex utilizes Mn as a catalyst for H₂O splitting in order to facilitate the formation of the higher valent oxidation states needed to promote the more difficult O−O bond forming step as well as reductive elimination of O₂. There would also be a closer energy match between the Mn(O(H)−H) and the biologically available TyrO−H bonds (Table 4), thereby facilitating an approximately thermoneutral process and avoiding unnecessary energy loss. This would of course require that Tyr−O• (Yz•), which was shown by a recent crystal structure to be a fair distance away from the Mn sites,[87] moves close enough to abstract a H atom from a Mn−(H)O−H during the reaction dynamics.

■ ASSOCIATED CONTENT

Ⓢ Supporting Information

ESI-MS data for **1**; quantitative UV−vis spectra of **1**, **8**, and **9** in MeCN; inverse variable magnetic susceptibility versus temperature data and fits for **9**; UV−vis spectrum of titration of **8** with HBF₄ (aq) followed by NH₄OH in MeCN; cyclic voltammograms for **2** and **3** in MeCN; infrared spectra of **1** and deuterated **1**; crystallographic data for **1**, **8**, and **9**. This material is available free of charge via the Internet at http://pubs.acs.org.

■ AUTHOR INFORMATION

Corresponding Author
*kovacs@chem.washington.edu

Notes
The authors declare no competing financial interest.

■ ACKNOWLEDGMENTS

■ REFERENCES

(1) Yano, J.; Kern, J.; Sauer, K.; Latimer, M.; Pushkar, Y.; Biesiadka, J.; Loll, B.; Saenger, W.; Messigner, J.; Zouni, A.; Yachandra, V. K. *Science* **2006**, *314*, 821−825.

(2) Dismukes, G. C.; Brimblecombe, R.; Felton, G. A. N.; Pryadun, R. S.; Sheats, J. E.; Spiccia, L.; Swiegers, G. F. *Acc. Chem. Res.* **2009**, *42*, 1935−1943.

(3) Yachandra, V. K.; Sauer, K.; Klein, M. P. *Chem. Rev.* **1996**, *96*, 2927−2950.

(4) Lewis, N. S.; Nocera, D. G. *Proc. Natl. Acad. Sci., U.S.A.* **2006**, *103*, 15729−15735.

(5) Nocera, D. G. *Acc. Chem. Res.* **2012**, 767−776.

(6) Kanan, M. W.; Nocera, D. G. *Science* **2008**, *321*, 1072−1075.

(7) Chen, Z.; Concepcion, J. J.; Jurss, J. W.; Meyer, T. J. *J. Am. Chem. Soc.* **2009**, *131*, 15580−15581.

(8) Concepcion, J. J.; Jurss, J. W.; Templeton, J. L.; Meyer, T. J. *J. Am. Chem. Soc.* **2008**, *130*, 16462−16463.

(9) Warren, J. J.; Tronic, T. A.; Mayer, J. M. *Chem. Rev.* **2010**, *110*, 6961−7001.

(10) Hashiguchi, B. G.; Bischof, S. M.; Konnick, M. M.; Periana, R. A. *Acc. Chem. Res.* **2012**, *45*, 885−898.

(11) Hoganson, C. W.; Babcock, G. T. *Science* **1997**, *277*, 1953−1957.

(12) Coggins, M. K.; Zhang, M.-T.; Vannucci, A. K.; Dares, C. J.; Meyer, T. J. *J. Am. Chem. Soc.* **2014**, *136*, 5531−5534.

(13) Ashford, D. L.; Song, W.; Concepcion, J. J.; Glasson, C. R. K.; Brennaman, M. K.; Norris, M. R.; Fang, Z.; Templeton, J. L.; Meyer, T. J. *J. Am. Chem. Soc.* **2012**, *134*, 19189−19198.

(14) Gupta, R.; Borovik, A. S. *J. Am. Chem. Soc.* **2003**, *125*, 13234−13242.

(15) Warren, J. J.; Mayer, J. M. *J. Am. Chem. Soc.* **2008**, *130*, 2774−2776.

(16) Roth, J. P.; Mayer, J. M. *Inorg. Chem.* **1999**, *38*, 2760−2761.

(17) Cowley, R. E.; BOntchev, R. P.; Sorrell, J.; Sarrancino, O.; Feng, Y.; Wang, H.; Smith, J. M. *J. Am. Chem. Soc.* **2007**, *129*, 2424−2425.

(18) Stone, K. L.; Borovik, A. S. *Curr. Opin. Chem. Biol.* **2009**, *13*, 114−118.

(19) Parsell, T. H.; Behan, R. K.; Green, M. T.; Hendrich, M. P.; Borovik, A. S. *J. Am. Chem. Soc.* **2006**, *128*, 8728−8729.

(20) Wang, K.; Mayer, J. M. *J. Am. Chem. Soc.* **1997**, *119*, 1470−1471.

(21) Usharani, D.; Lacey, D. C.; Borovik, A. S.; Shaik, S. *J. Am. Chem. Soc.* **2013**, *135*, 17090−17104.

(22) Rittle, J.; Green, M. T. *Science* **2010**, *330*, 933−937.

(23) Green, M. T. *Curr. Opin. Chem. Biol.* **2009**, *13*, 84−88.

(24) Denisov, I. G.; Makris, T. M.; Sligar, S. G.; Schlichting, I. *Chem. Rev.* **2005**, *105*, 2253−2277.

(25) Mak, P. J.; Denisov, I. G.; Victoria, D.; Makris, T. M.; Deng, T.; Sligar, S. G.; Kincaid, J. R. *J. Am. Chem. Soc.* **2007**, *129*, 6382−6283.

(26) Tinberg, C. E.; Lippard, S. J. *Acc. Chem. Res.* **2011**, *44*, 280−288.

(27) Brunold, T. C. *Proc. Natl. Acad. Sci., U.S.A.* **2007**, *104*, 20641−20642.

(28) Kodera, M.; Kawahara, Y.; Hitomi, Y.; Nomura, T.; Ogura, T.; Kobayashi, Y. *J. Am. Chem. Soc.* **2012**, *134*, 13236−13239.

(29) Oliw, E. H.; Jerneren, F.; Hoffmann, I.; Sahlin, M.; Garscha, U. *Biochim. Biophys. Acta* **2011**, *1811*, 138−147.

(30) Gilbert, N. C.; Bartlett, S. G.; Waight, M. T.; Neau, D. B.; Boeglin, W. E.; Brash, A. R.; Newcomer, M. E. *Science* **2011**, *331*, 217−219.

(31) Neidig, M. L.; Wecksler, A. T.; Schenk, G.; Holman, T. R.; Solomon, E. I. *J. Am. Chem. Soc.* **2007**, *129*, 7531−7537.

(32) Clark, K. B.; Culshaw, P. N.; Griller, D.; Lossing, F. P.; Simões, J. A. M.; Walton, J. C. *J. Org. Chem.* **1991**, *56*, 5535.

(33) Xu, S.; Mueser, T. C.; Marnett, L. J.; Funk, M. O., Jr. *Structure* **2012**, *20*, 1490−1497.

(34) Gillmor, S. A.; Villaseñor, A.; Fletterick, R.; Sigal, E.; Browner, M. F. *Nat. Struct. Biol.* **1997**, *4*, 1003−1009.

(35) Nelson, M. J. *J. Am. Chem. Soc.* **1988**, *110*, 2985−2986.

(36) Su, C.; Sahlin, M.; Oliw, E. H. *J. Biol. Chem.* **2000**, *275*, 18830−18835.

(37) Hamberg, M.; Su, C.; Oliw, E. *J. Biol. Chem.* **1998**, *273*, 13080−13088.

(38) Borovik, A. S. *Acc. Chem. Res.* **2005**, *38*, 54−61.

(39) Ogo, S.; Wada, S.; Watanabe, Y.; Iwase, M.; Wada, A.; Harata, M.; Jitsukawa, K.; Masuda, H.; Einaga, H. *Angew. Chem., Int. Ed.* **1998**, *37*, 2102−2104.

(40) Ogo, S.; Yamahara, R.; Roach, M.; Suenobu, T.; Aki, M.; Ogura, T.; Kitagawa, T.; Masuda, H.; Fukuzumi, S.; Watanabe, Y. *Inorg. Chem.* **2002**, *41*, 5513−5520.

(41) Yin, G. *Acc. Chem. Res.* **2013**, *46*, 483−492.

(42) Wang, Y.; Sheng, J.; Shi, S.; Zhu, D.; Yin, G. *J. Phys. Chem. C* **2012**, *116*, 13231−13239.

(43) Yin, G.; Danby, A. M.; Kitko, D.; Carter, J. D.; Scheper, W. M.; Busch, D. H. *J. Am. Chem. Soc.* **2008**, *130*, 16245−16253.

(44) Yin, G.; Danby, A. M.; Kitko, D.; Carter, J. D.; Scheper, W. M.; Busch, D. H. *J. Am. Chem. Soc.* **2007**, *129*, 1512−1513.

(45) Krebs, C.; Fujimori, D. G.; Walsh, C. T.; Bollinger, J. M., Jr. *Acc. Chem. Res.* **2007**, *40*, 484−492.

(46) Arunkumar, C.; Lee, Y.-M. M.; Lee, J. Y.; Fukuzumi, S.; Nam, W. *Chem.—Eur. J.* **2009**, *15*, 11482−11489.

(47) Wang, D.; Zhang, M.; Buhlmann, P.; Que, L., Jr. *J. Am. Chem. Soc.* **2010**, *132*, 7638−7644.

(48) Lansky, D. E.; Goldberg, D. P. *Inorg. Chem.* **2006**, *45*, 5119−5125.

(49) Bordwell, F. G.; Cheng, J.-P.; Harrelson, J. A., Jr. *J. Am. Chem. Soc.* **1988**, *110*, 1229−1231.

(50) Bordwell, F. G.; Cheng, J.-P.; Ji, G. Z.; Zhang, R. *J. Am. Chem. Soc.* **1991**, *113*, 9790−9794.

(51) Mayer, J. M. *Acc. Chem. Res.* **2011**, *44*, 36−46.

(52) Wayner, D. M.; Parker, V. D. *Acc. Chem. Res.* **1993**, *26*, 287−294.

(53) Tilset, M. In *Electron Transfer in Chemistry*; Balzani, V., Ed.; Wiley-VCH: Weinheim, Germany, 2001; pp 677−713.

(54) Coggins, M. K.; Brines, L. M.; Kovacs, J. A. *Inorg. Chem.* **2013**, *52*, 12383−12393.

(55) Behan, R. K.; Hoffart, L. M.; Stone, K. L.; Krebs, C.; Green, M. T. *J. Am. Chem. Soc.* **2006**, *128*, 11471−11474.

(56) Stone, K. L.; Behan, R. K.; Green, M. T. *Proc. Natl. Acad. Sci., U.S.A.* **2006**, *103*, 12307−12310.

(57) Green, M. T.; Dawson, J. H.; Gray, H. B. *Science* **2004**, *304*, 1653−1656.

(58) Hagen, K. S. *Inorg. Chem.* **2000**, *39*, 5867−5869.

(59) Evans, D. A. *J. Chem. Soc.* **1959**, 2005.

(60) Live, D. H.; Chan, S. I. *Anal. Chem.* **1970**, *42*, 791.

(61) Van Geet, A. L. *Anal. Chem.* **1968**, *40*, 2227−2229.

(62) Pistorius, E. K.; Axelrod, B. *J. Biol. Chem.* **1974**, *249*, 3183−3186.

(63) Prigge, S. T.; Boyington, J. C.; Faig, M.; Doctor, K. S.; Gaffney, B. J.; Amzel, L. M. *Biochimie* **1997**, *79*, 629−636.

(64) Hamor, M. J.; Hamor, T. A.; Hoard, J. L. *Inorg. Chem.* **1964**, *3*, 34−43.

(65) Coucouvanis, D.; Reynolds, R. A.; Dunham, W. R. *J. Am. Chem. Soc.* **1995**, *117*, 7570−7571.

(66) Kolnaar, J. J. A.; van Dijk, G.; Kooijman, H.; Spek, A. L.; Ksenofontov, V. G.; Gutlich, P.; Haasnoot, J. G.; Reedijk, J. *Inorg. Chem.* **1997**, *36*, 2433−2440.

(67) Mansuy, D.; Lange, M.; Chottard, J. C.; Bartoli, J. F.; Chevrier, B.; Weiss, R. *Angew. Chem., lnt. Ed.* **1978**, *17*, 780−781.

(68) Brines, L. M.; Shearer, J.; Fender, J. K.; Schweitzer, D.; Shoner, S. C.; Barnhart, D.; Kaminsky, W.; Lovell, S.; Kovacs, J. A. *Inorg. Chem.* **2007**, *46*, 9267−9277.

(69) Shearer, J.; Fitch, S. B.; Kaminsky, W.; Benedict, J.; Scarrow, R. C.; Kovacs, J. A. *Proc. Natl. Acad. Sci., USA* **2003**, *100*, 3671−3676.

(70) Shearer, J.; Scarrow, R. C.; Kovacs, J. A. *J. Am. Chem. Soc.* **2002**, *124*, 11709−11717.

(71) Shearer, J.; Nehring, J.; Kaminsky, W.; Kovacs, J. A. *Inorg. Chem.* **2001**, *40*, 5483−5484.

(72) Brines, L. M.; Villar-Acevedo, G.; Kitagawa, T.; Swartz, R. D.; Lugo-Mas, P.; Kaminsky, W.; Benedict, J. B.; Kovacs, J. A. *Inorg. Chim. Acta* **2008**, *361*, 1070−1078.

(73) MacBeth, C. E.; Golombek, A. P.; Young, V. G., Jr.; Yang, C.; Kuczera, K.; Hendrich, M. P.; Borovik, A. S. *Science* **2000**, *289*, 938−941.

(74) Yeh, C. Y.; Chang, C. J.; Nocera, D. G. *J. Am. Chem. Soc.* **2001**, *123*, 1513−1514.

(75) Groni, S.; Hureau, C.; Guillot, R.; Blondin, G.; Blain, G.; Anxolabehere-Mallart, E. *Inorg. Chem.* **2008**, *47*, 11783−11797.

(76) Goldsmith, C. R.; Stack, T. D. P. *Inorg. Chem.* **2006**, *45*, 6048−6055.

(77) Goldsmith, C. R.; Cole, A. P.; Stack, T. D. P. *J. Am. Chem. Soc.* **2005**, *127*, 9904−9912.

(78) Coggins, M. K.; Toledo, S.; Shaffer, E.; Kaminsky, W.; Shearer, J.; Kovacs, J. A. *Inorg. Chem.* **2012**, *51*, 6633−6644.

(79) Coggins, M. K.; Toledo, S.; Kovacs, J. A. *Inorg. Chem.* **2013**, *52*, 13325−13331.

(80) Kurtz, D. M., Jr. *Chem. Rev.* **1990**, *90*, 585−606.

(81) Baldwin, M. J.; Stemmler, T. L.; Reggs-Gelasco, P. J.; Kirk, M. L.; Penner-Hahn, J. E.; Pecoraro, V. L. *J. Am. Chem. Soc.* **1994**, *116*, 11349−11356.

(82) Armstrong, W. H.; Lippard, S. J. *J. Am. Chem. Soc.* **1984**, *106*, 4632−4633.

(83) Jullien, J.; Juhász, G.; Mialane, P.; Dumas, E.; Mayer, C.; Marrot, J.; Rivière, E.; Bominaar, E.; Münck, E.; Sécheresse, F. *Inorg. Chem.* **2006**, *45*, 6922−6927.

(84) Shearer, J.; Nehring, J.; Lovell, S.; Kaminsky, W.; Kovacs, J. *Inorg. Chem.* **2001**, *40*, 5483−5484.

(85) Gardner, K. A.; Kuehnert, L. L.; Mayer, J. M. *Inorg. Chem.* **1997**, *36*, 2069−2078.

(86) Baldwin, M. J.; Pecoraro, V. L. *J. Am. Chem. Soc.* **1996**, *118*, 11325−11326.

(87) Umena, Y.; Kawakami, K.; Shen, J.-R.; Kamiya, N. *Nature* **2011**, *473*, 55−61.